DOI: 10.13009/EUCASS2023-367
Aerospace Europe Conference 2023 – 10TH EUCASS – 9TH CEAS

Derivation of Buckling Knockdown Factors for Hemispherical Foam Core Shells

Chang-Hoon Sim, Chang-Min Lee, Gi-Seop Kim, and Jae-Sang Park†
Chungnam National University, Department of Aerospace Engineering

sch91@cnu.ac.kr – on8915@o.cnu.ac.kr – buffon5534607@o.cnu.ac.kr – aerotor@cnu.ac.kr
† Corresponding Author

Abstract

Nonlinear postbuckling analyses are performed to derive the buckling knockdown factor (KDF) for hemispherical foam core shells under external pressure. The commercial finite element analysis program, ABAQUS, is used for the postbuckling analyses. Two hemispherical foam core shells with different inner sheet thicknesses are considered. The crushable foam modeling technique is used to represent the nonlinear compressive behaviours of a foam material. The geometric initial imperfection is modeled using the single dimple imperfection. The present KDFs can provide the lightweight design of the hemispherical foam core shells.

1. Introduction

Lightweight design is important for space launch vehicles; in particular, the structural weight reduction for the propellant tank is quite important because it is the heaviest component in the launch vehicle structure. Therefore, several attempts have been made to reduce the structural weight of the propellant tank. One of the attempts is the use of a common bulkhead tank as shown in Fig. 1(a). The conventional propellant tank consists of the oxidizer tank, the interstage, and the fuel tank (Fig. 1(b)). On the other hand, the common bulkhead propellant tank uses a single tank with a common bulkhead that is designed as a hemispherical or elliptical shell. Because of this structural simplification, the common bulkhead propellant tank is lighter than a conventional propellant tank. However, the oxidizer and fuel regions in the common bulkhead tank are in close proximity to each other; therefore, the common bulkhead tank is susceptible to thermal insulation and buckling due to the thermal and pressure differences between the two regions. To solve this problem, a foam core sandwich structure is used as the hemispherical or elliptical shaped common bulkhead structure. The foam core sandwich provides excellent thermal insulation performance and a high structural stiffness to weight ratio. However, the foam material exhibits the nonlinear compressive behaviour, which makes it difficult to predict the buckling behaviour of foam core sandwich structures. In addition, the actual thin-walled shell structure includes initial imperfections that further complicate the prediction of the buckling behaviors. The initial imperfection of thin-walled shells significantly reduces the global buckling load. Therefore, the global buckling load of the thin-walled shell with the initial imperfection ($N_{imperfect}$) is lower than that of the perfect shell without an initial imperfection ($N_{perfect}$). This load reduction must be considered when designing the thin-walled shell structure of launch vehicles, which should withstand significant axial compressive loads. Therefore, the buckling design criterion, KnockDown Factor (KDF, γ), is used in the preliminary design phase of these structures to consider the buckling load reduction owing to the initial imperfection. The KDF is defined as the ratio between the global buckling loads of thin-walled shells with and without initial imperfections as given in Eq. (1). The lower the KDF, the heavier and more conservative the shell structure. Two buckling design criteria for hemispherical shells, SP-8032 [1] and CR-1457 [2], were established by NASA as shown in Fig. 2. NASA SP-8032 [1] was derived using various buckling test results for hemispherical shells from the 1930s-60s; thus, it cannot take into account modern technologies for manufacturing and materials. In addition, NASA SP-8032 [1] cannot provide the appropriate buckling design criteria for foam core shells because limited buckling test results for the foam core shells were used. Another design criterion, CR-1457 [2], used an analytical approach with test data to provide the buckling design criteria for foam core shells. However, there was a lack of test data to derive a reliable criterion for the foam core shell. Therefore, two previous buckling criteria [1, 2] may provide overly conservative designs for foam core shells.

$$\text{Buckling knockdown factor}, \gamma = \frac{N_{imperfect}}{N_{perfect}} \quad \textbf{(1)}$$

DOI: 10.13009/EUCASS2023-367

The experimental and numerical studies were performed to update the KDF for hemispherical shells under external pressure [3-6]. These studies [3-6] measured the global buckling loads of the metallic hemispherical shells, and compared test results with the numerical analysis results. The finite element models in these studies [3-6] considered the measured geometric data from the test articles to represent the geometric initial imperfection of the hemispherical shells However, it is impossible to use the measured initial imperfection in the preliminary design phase using the KDF. Therefore, numerical studies were performed to establish and validate the numerical initial imperfection modeling techniques for the metallic curved shells [7-9]. The different initial imperfection techniques were considered, such as the cut-out [7], mode shape imperfection [7], localized reduced stiffness method [8, 9], and dimple imperfection [9]. These imperfection modeling techniques were applied to the curved metallic shells with various shapes: hemispherical [7, 9], spherical [8], elliptical [7-9], and tori-spherical shells [7-9]. The previous studies [3-9] were conducted in-depth investigations on the metallic shell. However, the research for the derivation of the KDF of the foam core shell has not been reported.

In this study, numerical analyses are performed using ABAQUS to derive the KDF for the hemispherical foam core shells under external pressure. The crushable foam modeling method in ABAQUS is used to represent the nonlinear compressive behaviour of a foam material. The present modeling and analysis techniques are validated against the test results for the hemispherical shells in the reference [10]. In addition, the numerical initial imperfection modeling technique using a hemispherical rigid shell is introduced to represent the geometric initial imperfection of a hemispherical foam core shell. Then, the postbuckling analysis for the hemispherical foam core shell with the geometric initial imperfection is performed using the Riks method when the external pressure is applied. Finally, the KDFs are derived from the postbuckling analysis results with and without initial imperfections.

(a) Common bulkhead tank (b) Conventional propellant tank

Figure 1: Propellant tanks of space launch vehicles

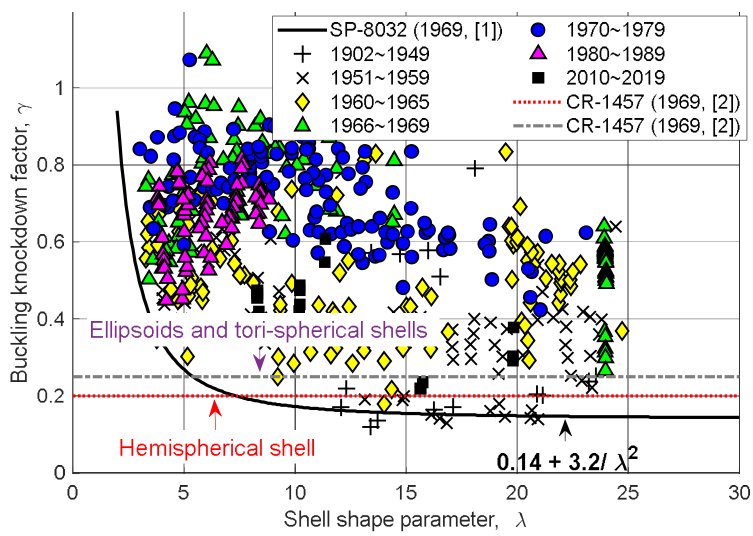

Figure 2: NASA's buckling design criteria

DOI: 10.13009/EUCASS2023-367

2. Methods

2.1 Nonlinear compressive behaviours of the foam material

Figure 3 shows the true stress-strain curve of the polymer foam material from a compression test [10]. There are three regions which indicate the linear elasticity, stress-plateau, and densification [11]. When a compressive load is applied to the foam material, the cell walls begin to bend, resulting in the linear elastic behaviour within the small strains. After the linear elastic behaviour, the stress does not increase with increasing the strains due to the buckling of the cell walls in a foam (stress plateau). As the compressive load continues to increase, the cell walls collapse, and the stress rapidly increases with increasing the strains (densification). This nonlinear compressive behaviour of foam materials must be considered in the finite element modeling of the foam core shell in order to predict the buckling behaviour of foam core shell structures. Therefore, the crushable foam modeling technique in ABAQUS is used for the hemispherical foam core shells in this study. The crushable foam modeling can take into account both the nonlinear compressive behaviour of foam materials and the foam hardening by densification [12].

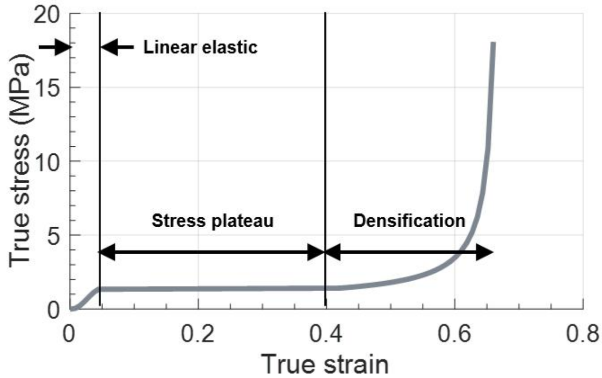

Figure 3: True stress-strain curve of the PVC80 foam from a compression test [10]

2.2 Analysis models and finite element modeling techniques

Two test articles of the hemispherical foam core shells from the previous study [10] are used as the present analysis models (Figure 4). The flat model and the dimple model have the inner sheet thickness of 0.42 and 0.40 mm (Fig. 4(a)), respectively. The geometric dimensions of the two analysis models are the same except for the inner sheet thickness. The face sheets and foam core are made of 201 stainless steel and PVC80 foam, respectively. The detailed material properties for the plasticity of stainless steel and PVC80 foam are obtained from the previous study [10], and are described in Table 1 and Fig. 5. The bottom edges of the two present models are clamped. The external pressure is represented by a uniformly distributed load. The foam core is modeled using the three dimensional (3D) solid elements with an element size of 1.54 mm to consider the large volume change due to the nonlinear compressive behaviours of foam materials (Fig 4(b)). The surface sheets are modeled using continuum shell elements with an element size of 1.04 mm to consider the contact between the outer sheet and the rigid plate that is used in the validation analysis (Fig 4(b)). The validation analysis for the finite element modeling using the crushable foam modeling technique will be discussed in Section 3.1. The surface sheets and the foam core are combined using the tie constraint.

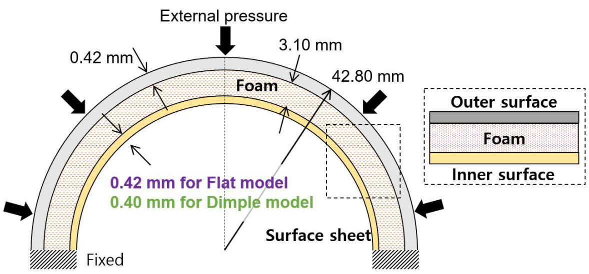

(a) Hemispherical foam core shell model [10]

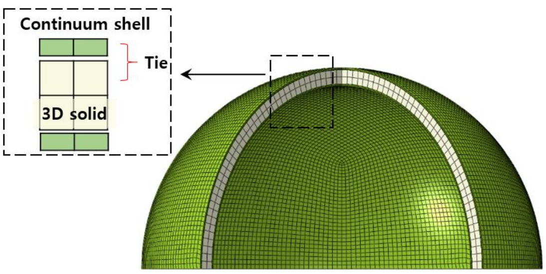

(b) Finite element model

Figure 4: Analysis models for hemispherical form core shell

DOI: 10.13009/EUCASS2023-367

Table1: Material properties [10]

	PVC80 foam	Stainless steel
Elastic modulus	0.04 GPa	210 GPa
Poisson's ratio	0.00	0.33
Density	80 kg/m^3	7,850 kg/m^3

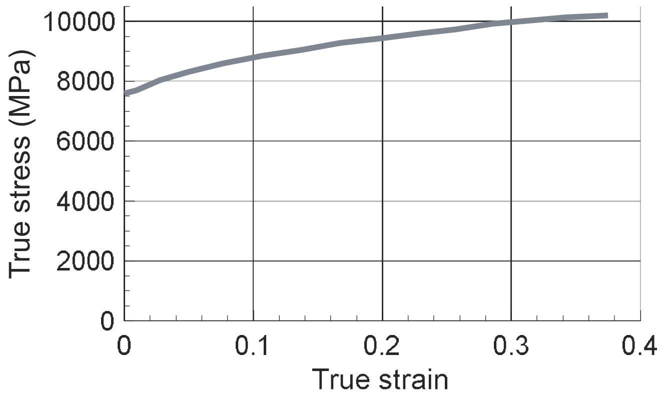

Figure 5: True stress-strain curve of the stainless steel from a tensile test [10]

2.2 Initial imperfection modeling: single dimple imperfection method

In this study, the geometric initial imperfection modeling technique, the single dimple imperfection method, is numerically introduced based on the Single Perturbation Load Approach (SPLA, [13]). The SPLA provides the realistic initial geometric imperfection of the thin-walled shell structure without a foam core [13]. In the SPLA, a single dimple, which is considered to be a realistic initial geometric imperfection, is modeled using a perturbation load. The foam core shell has large deformations due to the unique characteristic of foam materials; thus, the finite element model of the foam core shell is constructed using the solid element to consider the large deformation. Therefore, when the concentrated load, a perturbation load, is applied to the solid elements for the foam core, the mesh quality may be degraded by the localized large deformation [12]. Therefore, the hemispherical rigid shell is used to model the single dimple imperfection instead of a perturbation load to avoid the mesh quality degradation in finite element analyses. Figure 6 shows the initial imperfection modeling technique for the hemispherical shell with the foam core. The radius of the hemispherical rigid shell is assumed as 10% of the radius of the flat and dimple models. The hemispherical rigid shell is modeled using the analytical rigid, and the transverse enforced displacement is applied to the reference point of a hemispherical rigid shell. The Newton-Raphson method is applied to obtain the initial geometric imperfection from the single dimple imperfection method. The surface to surface contact method is used to represent the contact behaviour between the foam core shell and the hemispherical rigid shell. As shown in Fig. 7, the global buckling load of a foam core shell with the single dimple imperfection ($N_{imperfect}$) decreases as the single dimple imperfection magnitudes increase. However, the $N_{imperfect}$ converges, when the magnitudes of the dimple imperfections exceed a certain level. The KDF is derived using the converged global buckling load ($N_{imperfect}$) and the linear buckling load of a perfect foam core shell without the initial imperfection. The nondimensional value, μ, is used to express the magnitudes of the single dimple imperfections. As given in Eq. (2), the μ is defined as the ratio between the magnitudes of the single dimple imperfections and the total thickness of the foam core shells.

DOI: 10.13009/EUCASS2023-367

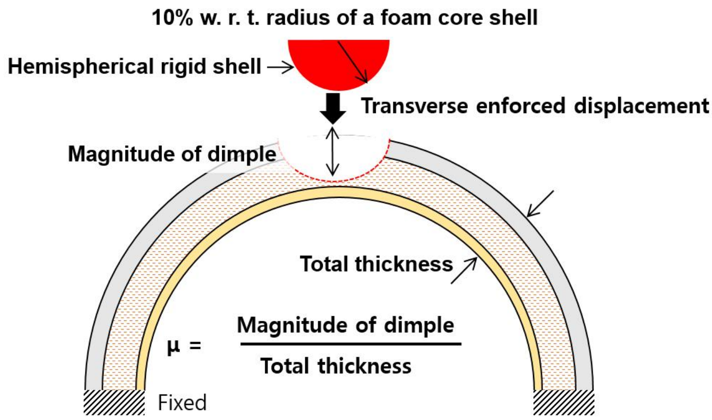

Figure 6: Single dimple imperfection modeling technique

$$\mu = \frac{\text{Magnitude of dimple}}{\text{Total thickness}, t_{total}} \tag{2}$$

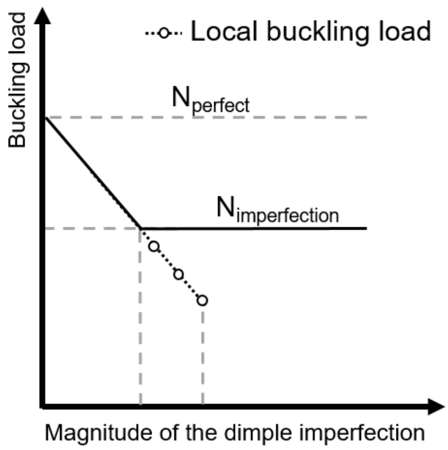

Figure 7: Convergence of the global buckling load in terms of the magnitude of the single dimple imperfection

2.3 Procedure of the postbuckling analysis of hemispherical foam core shells with the flat and dimple models

The postbuckling analysis is performed to derive the KDFs of the hemispherical foam core shells with the flat and dimple models. The analysis procedure consists of the initial imperfection modeling step and the postbuckling analysis step. In the first step, the geometric initial imperfection is modeled using the single dimple imperfection modeling technique. The deformed foam core shell due to the imperfection modeling is passed to the postbuckling analysis step without the pre-stresses. In the second step, the external pressure is applied to the deformed hemispherical foam core shells, and the buckling behaviours are predicted using the Riks method. The procedure of the postbuckling analysis is repeated by increasing the μ until the $N_{imperfect}$ converges.

3. Results and discussions

3.1 Validation study for finite element modeling techniques

The validation study is performed to establish the finite element modeling technique considering the nonlinear compressive behaviours of foam materials. Figure 8 indicates the method and result of the validation study of the finite element modeling technique. The validation analysis is conducted using the explicit scheme with a surface to surface contact method. The compressive load in the compression test [10] is replaced by the analytical rigid plate, which is subjected to the transverse enforced displacement (Fig. 8(a)). As shown in Fig. 8(b), in both cases of the compression

DOI: 10.13009/EUCASS2023-367

tests [10] and present results, the deformed shapes of the flat model are flatter than those of the dimple model. The difference in the inner sheet thickness of the flat and the dimple models causes this difference in the deformed shapes. In the compression test [10], the three-pointed star shape occurs in the deformed shapes of the flat and dimple models. However, in the present work, the deformed shapes of the flat and dimple models are observed as the four-pointed star shapes (plus sign shape). These differences in the two results between the compression test [10] and the present analysis may be due to the uncertainty in the test [10], such as the imperfect bond area of a foam core. The initial imperfection of the flat and dimple models is not considered in the validation study. However, the difference in the deformed shapes of the flat and dimple models is clearly observed in both the compression test [10] and the present work. In addition, the load-displacement curves obtained from the compression test [10] and the validation study are in good agreement. Therefore, the finite element modeling technique, which takes into account the nonlinear compressive behaviours of the foam material is well validated and established.

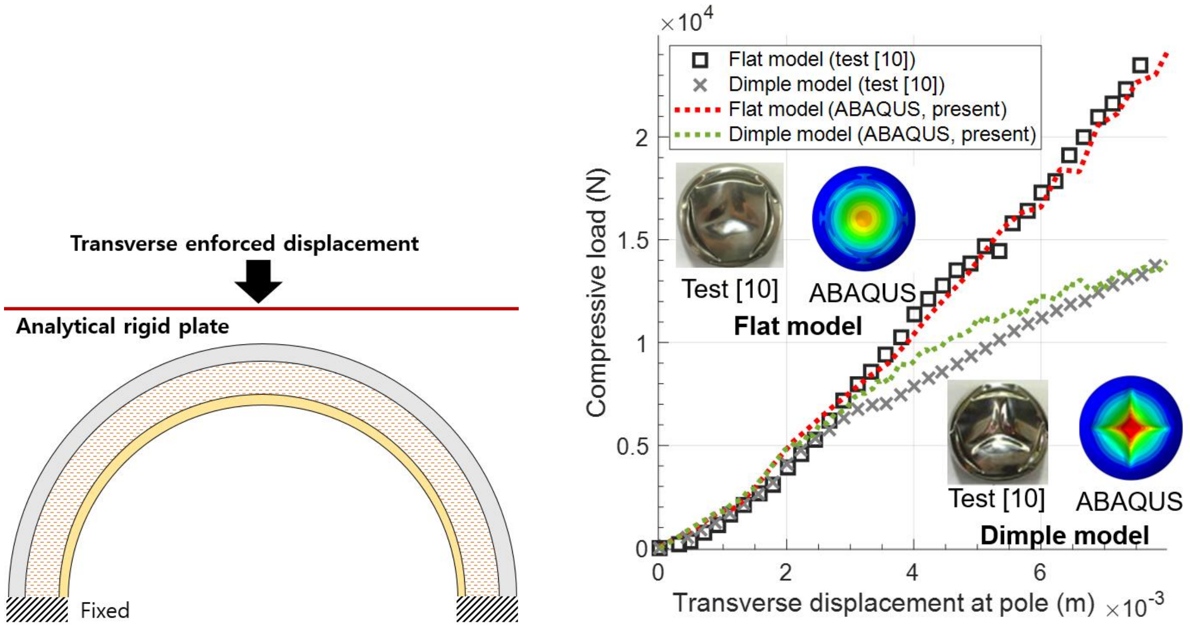

(a) Method

(b) Load-displacement curves for flat and dimple models

Figure 8: Method and results of the validation study

3.2 Postbuckling results

3.2.1 Flat model

This section describes the buckling analyses for the flat model with an inner sheet thickness of 0.42 mm. Figure 9 shows the postbuckling analysis results for the perfect model without the initial imperfection when the external pressure is applied. The transverse displacement is calculated at the pole of the hemispherical shell. The global buckling load obtained from the linear buckling analysis is 27.53 MPa. However, the global buckling load by the nonlinear postbuckling analysis is predicted to be 12.45 MPa, which is 54.78% lower than the linear buckling load. In general, the global buckling loads from the linear buckling and nonlinear postbuckling analyses for thin-walled shell structures are similar; thus, the geometric nonlinearity may not seriously affect the global buckling load. Therefore, the difference in the global buckling loads between the linear and nonlinear analyses in this study may be caused by the material nonlinearity such as plasticity. Consequently, the material nonlinearity such as plastic may cause the difference in the present global buckling loads between the linear and nonlinear analyses. As shown in this figure, the buckling shapes differ between the analysis results. In the linear buckling analysis, the buckling waves are distributed in the upper region of the foam core shell. On the other hand, in the postbuckling analysis, the buckling waves are observed at the bottom edge of the perfect model. These results indicate that the material nonlinearity influences the buckling behaviours of the hemispherical foam core shells. The reduction in the global buckling loads due to the material nonlinearity is difficult to be predicted in the preliminary design phase. Therefore, for the perfect model, the linear buckling load is used as the global buckling load for the model without initial imperfections, $N_{perfect}$ when the KDF is derived using Eq. (1).

DOI: 10.13009/EUCASS2023-367

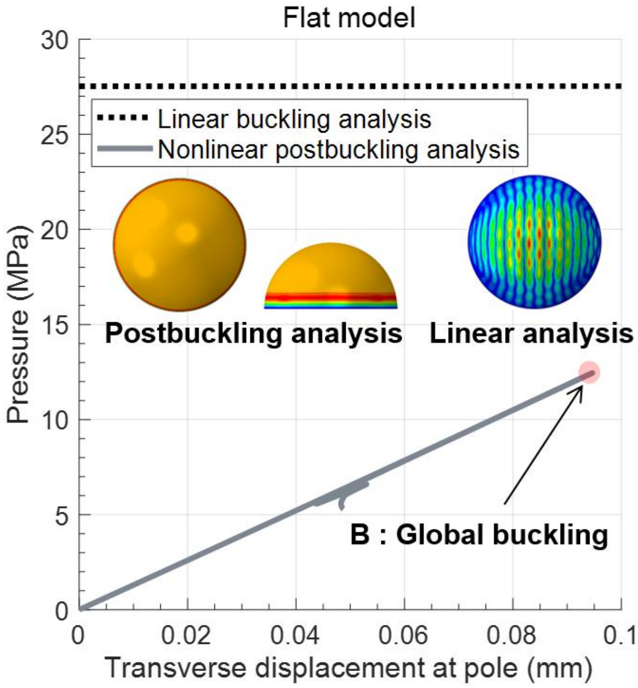

Figure 9: Buckling analysis results for the perfect flat model without the initial imperfection

The load-displacement curves of the flat models with different initial imperfection magnitudes are illustrated in Fig. 10. The transverse displacements of these curves are shifted in a positive direction by the magnitude of the single dimple imperfection. As the μ increases, the global buckling loads considering the initial imperfection ($N_{imperfect}$) decrease. However, $N_{imperfect}$ converges to 6.03 MPa when the μ exceeds 0.50. The local buckling (A) is observed clearly in cases of the μ = 0.25 and 0.50. As the μ increases to 0.75, the local buckling disappears. Figure 11 presents the deformed shapes of the flat models at μ = 0.25. As shown in Fig. 11(A), at the local buckling (A), only the outer sheet of the hemispherical foam core shells is buckled. However, at the global buckling (B), the entire foam core sandwich, including the outer/inner sheets and foam core, is buckled (Fig. 11(B)). The deformed shape in the postbuckling state (C) is similar to that in the global buckling, but the area of the dimple shape caused by the external pressure increases in the transverse and radial directions (Fig. 11(C)).

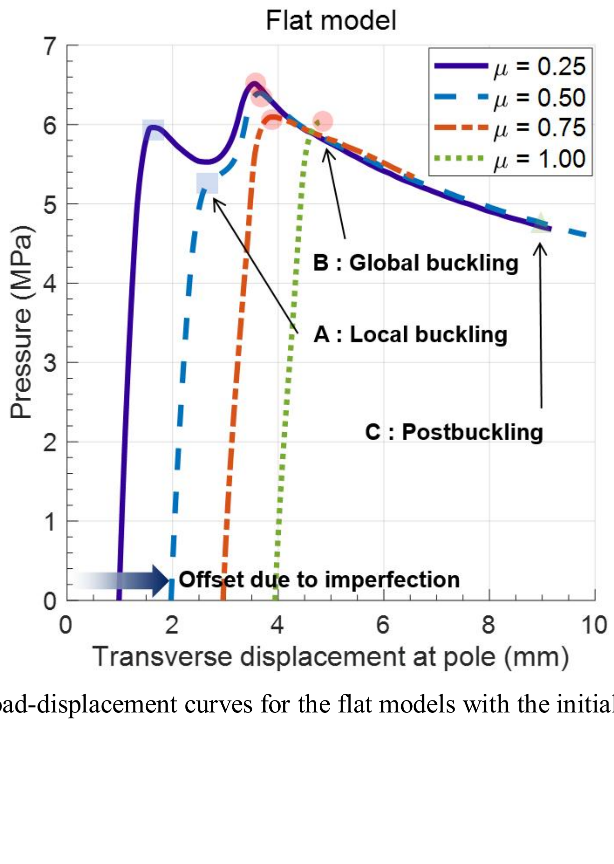

Figure 10: Load-displacement curves for the flat models with the initial imperfections

DOI: 10.13009/EUCASS2023-367

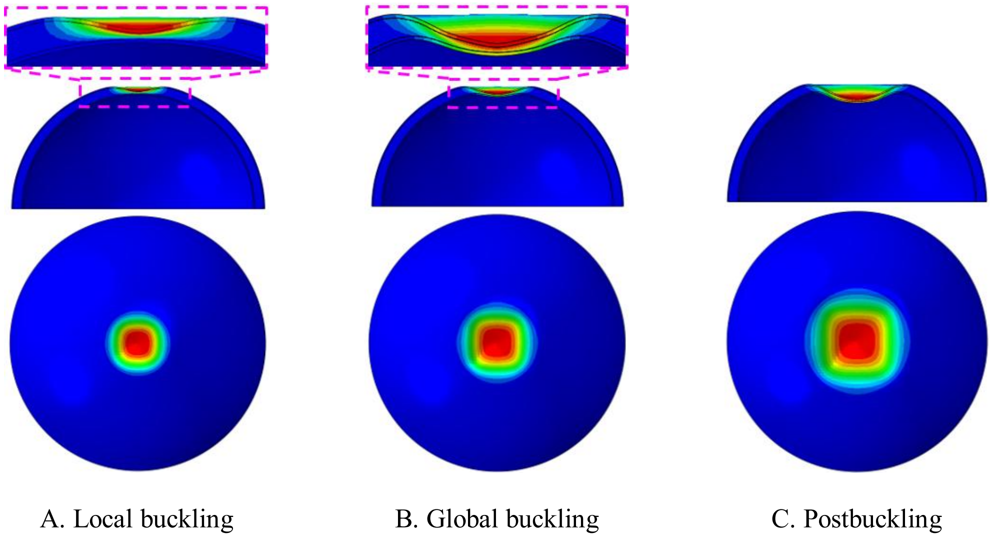

Figure 11: Deformed shapes of the flat model at μ = 0.25

3.2.2 Dimple model

The buckling analysis results for the dimple model without the initial imperfection are described in Fig. 12. The dimple model has an inner sheet thickness of 0.40 mm, which is 5% lower than that of the flat model. The global buckling loads using linear buckling analysis ($N_{perfect}$) and nonlinear postbuckling analysis are 27.56 and 12.44 MPa, respectively. Similar to the results of the flat model, the global buckling load obtained from the nonlinear analysis is 54.68% lower than the linear buckling load. In the linear buckling analysis results, the global buckling occurs with a checkerboard shape; however, in the nonlinear postbuckling analysis, the global buckling is observed with the ring shape near the bottom edge. The differences in buckling loads and shapes are due to the material nonlinearity as described previously.

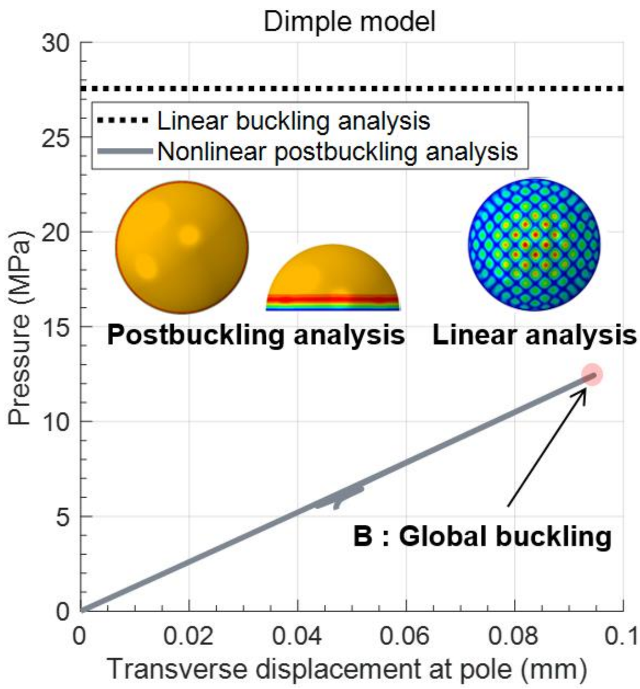

Figure 12: Buckling analysis results for the perfect dimple model without the initial imperfection

DOI: 10.13009/EUCASS2023-367

Figures 13 and 14 show the postbuckling analysis results of the dimple models with different initial imperfection magnitudes. As given in Fig. 13, the $N_{imperfect}$ is predicted to be 5.63 MPa when the μ exceeds 0.50. The local buckling (A) is observed in the curves at μ = 0.25 and 0.50. Similar to the results of the flat model in Fig. 10, the local buckling (A) does not occur when the μ is higher than 0.75. As the external pressure increases, only the outer sheet of the dimple model is buckled, and the local buckling (A) is observed (Fig. 14(A)). After the local buckling (A), the global buckling (B) occurs with the foam core and the inner sheet is buckled with the outer sheet (Fig. 14(B)). As the external pressure continues to increase, the area of the dimple shape increases in the transverse and radial directions (postbuckling, Fig. 11(C)).

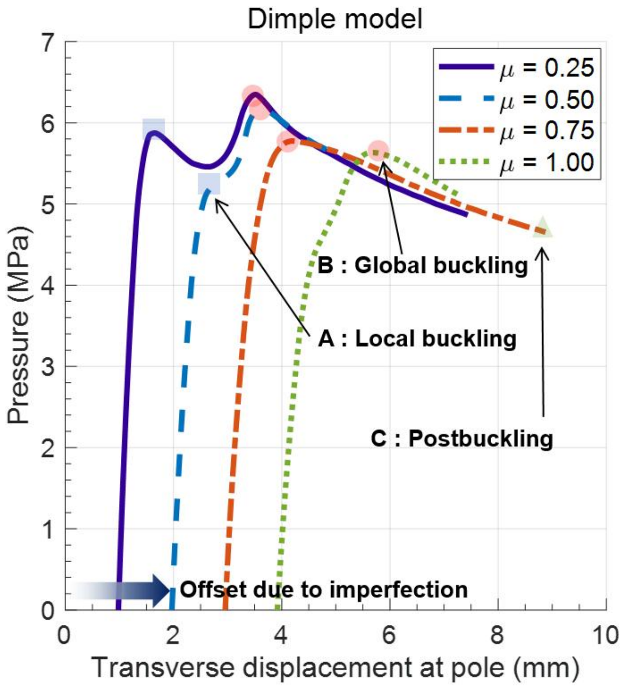

Figure 13: Load-displacement curves for the dimple models with the initial imperfections

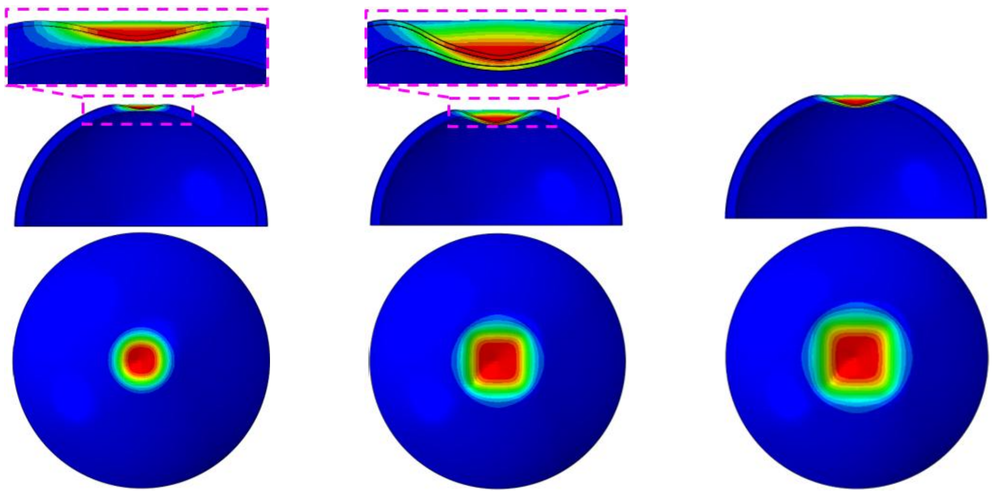

A. Local buckling B. Global buckling C. Postbuckling

Figure 14: Deformed shapes of the dimple model at μ = 0.25

DOI: 10.13009/EUCASS2023-367

3.3 Global buckling loads and buckling knockdown factors

Figure 15 shows results for global buckling loads of the flat and dimple models. As shown in this figure, the $N_{perfect}$ of the flat and dimple models, which are 27.53 and 27.56 MPa, respectively, are quite similar. However, the $N_{imperfect}$ of the flat model (6.03 MPa) is 7.10% higher than that of the dimple model (5.63 MPa). This difference in the $N_{imperfect}$ is due to the fact that the inner sheet thickness of the flat model is 5.00% thicker than that of the dimple model. Since the buckling stability of the perfect model is higher than that of the imperfection model, the effect of the inner sheet thickness is not clearly observed in the results for the perfect models ($N_{perfect}$). As given in Fig. 16, the KDF of the flat model is derived to be 0.22, which is 10.00% higher than the KDF of the dimple model (0.20). The KDF of the flat model is 22.22% and 10.00% higher than NASA SP-8032 (0.18, [1]) and CR-1457 (0.20, [2]), respectively. The KDF of the dimple model is 11.11% higher than NASA SP-8032 (0.18 [1]); however, it is equal to NASA CR-1457 (0.20, [2]). The following two reasons can cause these results. First the flat and dimple models both are the small-scale models, which are more sensitive to the geometric initial imperfection than large-scale structures [13, 14]. Second, as described previously, the previous buckling design criteria [1, 2] may not provide a suitable KDF for hemispherical foam core shells. Compared to NASA SP-8032 [1], two present KDFs can provide a lightweight design of the hemispherical foam core shells for common bulkhead structures. On the other hand, as compared to NASA CR-1457 [2], only the KDF of the flat model satisfies the lightweight design. Although the KDF of the dimple model and NASA CR-1457 [2] are the same, the other KDFs are higher than the previous buckling design criteria [1, 2]. Therefore, these results show that the buckling design criteria for the hemispherical foam core shells can be improved by in-depth numerical studies instead of buckling tests.

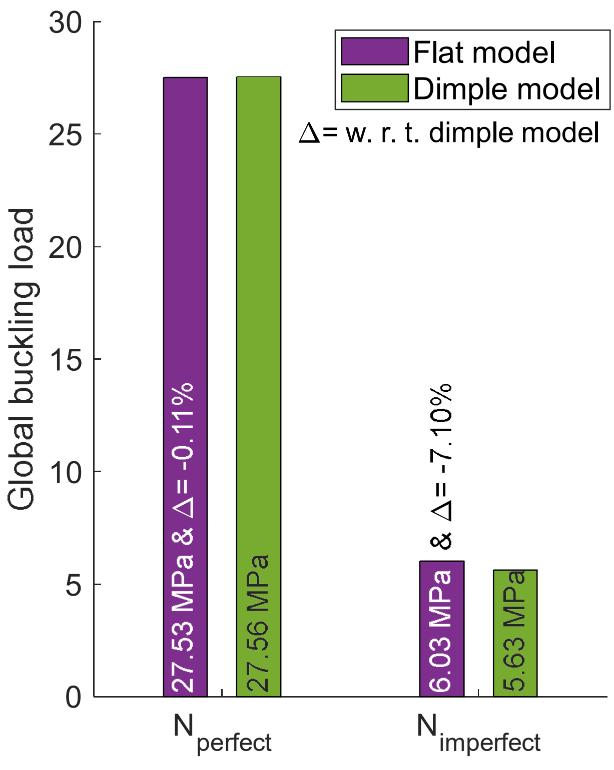

Figure 15: Global buckling loads

DOI: 10.13009/EUCASS2023-367

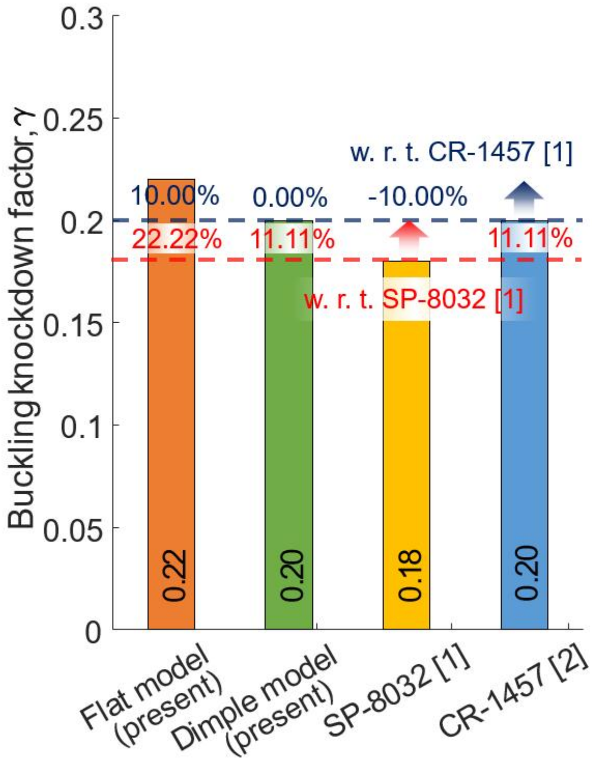

Figure 16: Buckling knockdown factors

4. Conclusions

In this study, the buckling KnockDown Factors (KDF) for hemispherical foam core shells were numerically derived using ABAQUS. The finite element modeling technique considering the nonlinear compressive behaviours of foam materials was established and validated in comparison with the previous compression tests using the flat and dimple models. The crushable foam modeling technique in ABAQUS was used to represent the nonlinear compressive behaviours of the PVC80 foam material. The postbuckling analyses using the Riks method were conducted for the hemispherical foam core shells under external pressure. The initial imperfection of the foam core shells was represented using the single dimple imperfection. The KDFs of the flat and dimple models were derived to be 0.22 and 0.20, respectively. The KDF of the flat model (0.22) was 22.22% and 10.00% higher than the NASA SP-8032 (0.18) and CR-1457 (0.20), respectively. However, the KDF of the dimple model (0.20) was 11.11% higher than NASA SP-8032 (0.18), and it was equal to CR-1457 (0.20). These results indicated that the less conservative KDFs for hemispherical foam core shells could be derived. However, it was noteworthy that the flat and dimple models with a radius of 41.80 mm in this work were small-scale models, which were more susceptible to the geometric initial imperfection than large-scale structures, such as the actual launch vehicle structures. Therefore, a numerical study for a large-scale model will be required to derive the robust KDF for the hemispherical foam core shell structures of launch vehicles.

References

[1] Weingarten, V. I. and Seide, P. 1969. Buckling of thin-walled doubly curved shells. NASA SP-8032.

[2] Sullins, R. T., Smith, G. W., and Spier, E. E. 1969. Manual for structural stability analysis of sandwich plates and shells. NASA CR-1457.

[3] Zhu, Y., Zhang, Y., Zhao, X., Zhang, J., and Xu, X. 2019. Elastic–plastic buckling of externally pressurised hemispherical heads. Ships and Offshore Structures. 14(8):829–838.

[4] Zhang, J., Wang, Y., Wang, F., amd Tang, W. 2018. Buckling of stainless steel spherical caps subjected to uniform external pressure. *Ships and Offshore Structures*. 13(7):779–785.

[5] Wang, Y., Tang, W., Zhang, J., Zhang, S., and Chen, Y. 2019. Buckling of imperfect spherical caps with fixed boundary under uniform external pressure. *Marine Structures*. 65:1–11.

DOI: 10.13009/EUCASS2023-367

[6] Zhang, J., Zhang, Y., Wang, F., Zhu, Y., Cui, W., Chen, Y., and Jiang, Z. 2019. Experimental and numerical studies on the buckling of the hemispherical shells made of maraging steel subjected to extremely high external pressure. *International Journal of Pressure Vessels and Piping*. 172:56–64.
[7] Wagner, H. N. R., Hühne, C., and Niemann, S. 2018. Robust knockdown factors for the design of spherical shells under external pressure: Development and validation. *International Journal of Mechanical Sciences*. 141:58–77.
[8] Wagner, H. N. R., Hühne, C., Zhang, J., Tang, W., and Khakimova, R. 2019. Geometric imperfection and lower-bound analysis of spherical shells under external pressure. *Thin-Walled Structures*. 143:106195.
[9] Wagner, H. N. R., Niewöhner, G., Pototzky, A., and Hühne, C. 2021. On the imperfection sensitivity and design of tori-spherical shells under external pressure. *International Journal of Pressure Vessels and Piping*. 191:104321.
[10] Wang, S., Li, S., and He, J. 2017. Buckling behavior of sandwich hemispherical structure considering deformation modes under axial compression. *Composite Structures*. 163:312–324.
[11] Gong, L., Kyriakides, S., and Jang, W. Y. 2005. Compressive response of open-cell foams. Part I: Morphology and elastic properties. *International Journal of Solids and Structures*. 42(56):1355–1379.
[12] Dassault Systémes Simulia Corp. 2013. Abaqus Users, Ver. 6.13-2, Dassault Systémes Simulia Corp.
[13] Singer, J., Abramovich, H. 1995. The development of shell imperfection measurement techniques. *Thin-walled structures*. 23:379–398.
[14] Teng, J. G. and Rotter, J. M. 2004. Buckling of thin metal shells. CRC Press.